Received: 29 May 2021 | Revised: 3 January 2022 | Accepted: 25 February 2022

IET Power Electronics

DOI: 10.1049/pel2.12275

The Institution of Engineering and Technology WILEY

ORIGINAL RESEARCH PAPER

An ultra-low-loss superconducting inductor for power electronic circuits

Xiaoyuan Chen[1] | Huayu Gou[1] | Yu Chen[1] | Lei Zeng[1] | Mingshun Zhang[1] | Shan Jiang[1] | Qi Xie[1] | Boyang Shen[2]

[1]School of Engineering, Sichuan Normal University, Chengdu, China

[2]Department of Engineering, University of Cambridge, Cambridge, UK

Correspondence
Boyang Shen, Department of Engineering, University of Cambridge, Cambridge CB3 0FA, United Kingdom.
Email: bs506@cam.ac.uk

Funding information
National Natural Science Foundation of China, Grant/Award Number: 51807128

Abstract

To break through the bottlenecks of the loss and size of conventional conductors and magnetic materials, replacing copper inductors by zero-resistance superconducting inductors can be a promising solution. The experimental, theoretical and numerical investigations into the loss characteristics of an air-core superconducting inductor have been carried out. All these results show that the loss from a superconducting inductor in the boost chopper circuit was reduced remarkably up to 373 times smaller than the loss from the magnetic-core copper inductor having the same conditions. Moreover, the actual volume and weight of the superconducting inductor are only 5.61% and 10.97% of those of the copper inductor having the same inductance and current capacities. Advanced numerical models have been built to verify the experiments that their results of superconducting losses as well as the current and frequency dependencies are well matched. A compact, low-loss and low-cost cryostat has been designed to accommodate the superconducting inductor, which can further improve the practicability for superconducting inductor to be equipped into various power electronic applications. The superconducting inductor can lead power electronic devices towards ultra-high-efficiency power conversion.

1 | INTRODUCTION

As one of the most common components of power electronic circuits, power inductor is widely used in diverse alternating-current (AC) and direct-current (DC) power conversion systems [1]. Specifically, various types of air-core and magnetic-core power inductors can be served as transient electromagnetic energy buffers, filters, oscillators, dampers etc. To properly control transient energy flow in the circuit, all the power inductors should be designed with a certain inductance and current ratings. Considering both the engineering current density and inherent resistivity of copper conductor, air-core inductor is suffered from the large size, heavy mass and high loss. In order to achieve a compact structure, various types of high-permeability magnetic cores are adopted. Compared to air-core inductors, the magnetic-core inductor having the same inductance capacity can be wound by a much smaller number of coil turns, resulting in an obvious decrease of unit size.

Considering the ever-increasing developments of clean and renewable energy sources all over the world in recent years, three principal performance requirements of power inductors used in various power electronic circuits are the small size, high current and low loss. For the operations of six basic DC-DC converters of Buck, Boost, Buck-Boost, Cuk, Sepic and Zeta, and a number of modified chopper circuits [2, 3], power inductors are generally controlled by a series of electronic power switches to charge and discharge repeatedly for implementing continuous electromagnetic energy interactions between high-voltage side and low-voltage side. However, high-frequency operations cause serious magnetic loss inside the cores and high copper loss inside the windings due to combined effects of hysteresis, eddy, skin and proximity phenomena. From an engineering application point of view, at present there are two main solutions which are using copper litz wires and optimizing magnetic core structure [4].

In addition to various low-loss inductor designs at room temperature, cryogenic operations of magnetic-core inductors have also been investigated as preliminary trials. It is found that magnetic losses generally increase as temperature decreases, and this counteracts the reduction in copper losses and the total

inductor loss is almost the same as its room-temperature value [5, 6]. Even worse, if the whole inductor is immersed into the cryogenic liquid nitrogen at 77 K, the real power dissipation to take away the heat generated should be multiplied by more than 10 times of the inductor loss occurs at cryogenic temperature. Even when the magnetic core is removed for forming an air-core inductor, copper resistivity can only be reduced by a factor of 5 from 300 to 77 K.

Fortunately, high temperature superconducting (HTS) inductor wound by zero-resistance superconductor is a great substitute for conventional copper unit at 77 K [7]. In Shanghai Superconductor Technology Co. Ltd., a commercial ReBCO tape with average width of 4.8 mm and average thickness of 0.33 mm has a typical critical current of 220 A at 77 K, corresponding to approximately 138.89 A/mm^2 without any conducting loss. By comparison, copper wire is normally with a resistivity of 0.02 $\mu\Omega$ m and a current density of 2 A/mm^2, resulting in a unit loss of 0.08 μW m/mm^2. Moreover, the benefit of high current density in HTS tape makes it available to wind a small-size inductor which involves no magnetic core at all. In theory, this superconducting inductor can be considered as an ideal inductor without both the copper loss and magnetic loss.

At present, benefited from the unique advantages of zero energy loss, high current density and compact device size, a great number of theoretical and experimental studies have done regarding superconducting coils/magnets (also can be regarded as power inductors). Prototypes have been investigated and used into large-scale power and energy systems such as superconducting magnetic energy storage [8], superconducting fault current limiter [9], superconducting power transformer [10], superconducting magnetic resonance imaging [11] and superconducting nuclear fusion [12], where the operating environments are with DC or relatively low frequencies such as 50/60 Hz. However, these large-scale superconducting inductors require fairly high capital cost and relatively large installation dimension. For most power electronics applications (operating frequency generally over 5000 Hz), the power inductors need relatively small inductance ranging from tens to hundreds of microhenry (μH), where the total cost of superconducting inductor will be much cheaper as less amount of superconducting material is needed. Therefore, a new combination of the compact superconducting inductor and the power electronic circuits can be well expected to achieve the high-efficiency and economic power conversions.

To break through the technological bottlenecks rooted from conventional conductors and magnetic materials, this paper presents the use of a highly efficient ultra-low-loss superconducting inductor. The characteristics of operating loss of a superconducting inductor prototype have been analysed based on both the experimental loss tests and simulations, which can clarify the feasibility and practicability of using this superconducting power electronic circuit towards an ultra-high-efficiency power conversion.

2 | THE LOSS MECHANISM OF SUPERCONDUCTOR

The superconducting materials are generally recognized as the perfect conductors which have the lossless behaviour. However, from engineering aspects, the practical superconducting tapes and coils suffer a certain amount of loss, particularly when they are involved in the AC system, for example, working with the AC magnetic field or AC transport current [13]. These losses are usually called the AC loss of superconductors. The total AC loss of HTS coils is normally composed of these losses: the hysteresis loss from superconducting layer, and the eddy-current loss in the metal (e.g., silver and copper) layers, which are the dominant losses in the state-of-the-art HTS wires, while the coupling loss and magnetic loss are much less significant in these wires [14]. There are several experimental methods, such as the electrical method, magnetic method and calorimetric method, which could measure particular losses, but when the complexity of system increases, these measurements will give rise to problematic interactions and become less efficient [15]. Therefore, a powerful numerical tool to simulate the accurate AC loss is essentially important. Based on our previous work [15, 16], the finite-element method (FEM) using the $\boldsymbol{H}$-formulation has been proved as one of the most reliable approaches to compute the AC loss from various complex superconducting systems, such as our supercomputing power conversion system.

Furthermore, the superconducting power conversion device in this article not only involved the conventional AC loss, but also encountered the superconducting dynamic loss [17]. This is a relatively deeper physics of a superconductor carrying a DC current and simultaneously in the presence of AC magnetic field, and then it induces an extra magnetic flux [18]:

$$\Delta\phi = \frac{2al\,I_a}{I_c}\left(B_a - B_{a,th}\right) \tag{1}$$

where I_c is the critical current of HTS tape, a and l are the width and length of HTS wires, $B_{a,th}$ is the threshold field, and the B_a is the half peak-peak value of the applied field and in this article it was induced by the triangle AC ripple signal from the power electronics. Fortunately the physics of superconducting dynamic loss can also be properly calculated by the $\boldsymbol{H}$-formulation [19]. Therefore the total loss in the HTS coil for this supercomputing power conversion system can be calculated as:

$$P_{total\ loss} = P_{ac\ loss} + P_{dynamic\ loss} + P_{inductive\ loss} \tag{2}$$

The modelling of Equation (2) can be carried out using the $\boldsymbol{H}$-formulation based on the FEM software COMSOL.

3 | EXPERIMENTAL INVESTIGATIONS

The air-core HTS inductor tested in this work is a single pancake coil wound by 20 coil turns. Its inner diameter, outer diameter,

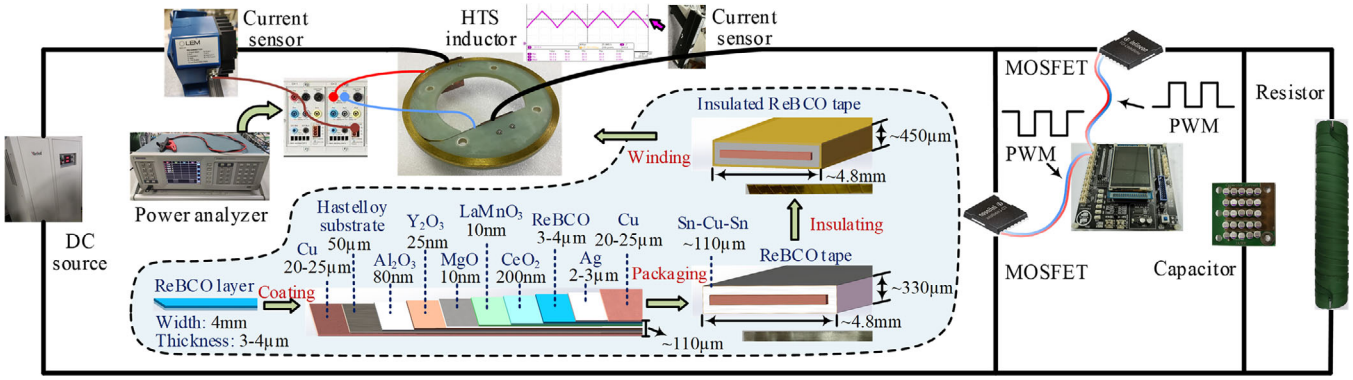

FIGURE 1 A boost chopper circuit to evaluate the loss characteristics of HTS ReBCO air-core inductor

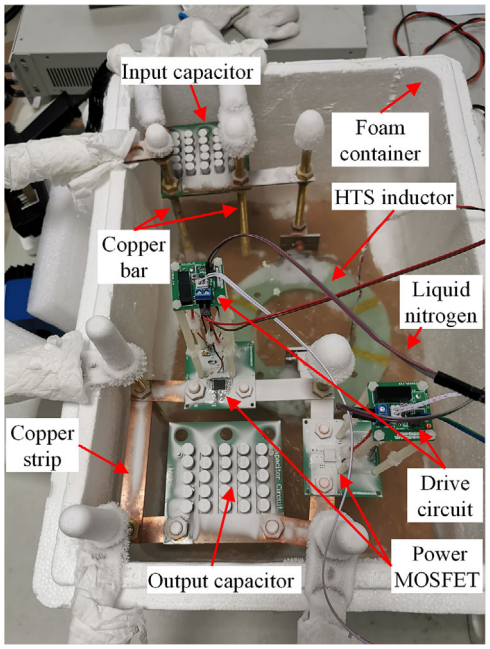

FIGURE 2 Prototype of the low-temperature boost chopper testing platform

thickness and height are about 200 mm, 219.2 mm, 9.6 mm and 4.8 mm, respectively. The total inductance L is about 203.44 μH. The entire preparation process of coating, packing, insulating and winding are presented in the dotted box in Figure 1.

To evaluate the loss characteristics of the air-core HTS inductor, a boost chopper testing circuit is built, as shown in Figure 2. The HTS inductor is installed inside a low-temperature container and fully immersed into the liquid nitrogen at 77 K. With the sufficient cooling capacity from the surrounding cryogenic refrigerant, the experimental inductor operates at superconducting state and exhibits zero resistance with DC. Two power MOSFETs and their equipped drive circuits are adopted to build a boost chopper module. Several low-loss copper strips and bars are used to connect different circuit elements and modules.

As for the control of the testing circuit, complementary PWM control signals are sent to two power MOSFETs for implementing a repeated charging and discharging operations

TABLE 1 Main electrical specifications of the boost chopper circuit

U_{in} (V)	I_{in} (A)	D	U_{out} (V)	I_{out} (A)	R (Ω)	P (W)
8.1	90	0.7	27	27	1	729
14.4	90	0.6	36	36	1	1296
22.5	90	0.5	45	45	1	2025
32.4	90	0.4	54	54	1	2916
44.1	90	0.3	63	63	1	3969

of the superconducting inductor. If ignoring tiny amount of line impedance and switching resistance, transient inductor current can be considered as a triangular wave with DC bias. In general, this DC bias current is also called the steady-state operating current. A current ripple factor K, which is defined as the ratio of peak triangular current I_{ac} to DC bias current I_{dc}, can be estimated by

$$K = \frac{I_{ac}}{I_{dc}} = \frac{RD(1-D)^2}{2fL} \tag{3}$$

where R is the load resistance, f and D are the switching frequency and duty cycle of PWM signal. This AC ripple estimation formula has been well proved by practical measurements. In the cases of f = 1, 2 and 3 kHz, the current ripple factors obtained from the experimental inductor currents in Figure 3 are about 0.32, 0.17 and 0.12, respectively. These experimental deviations are less than 0.02 as compared to their corresponding ideal values in (3).

During the tests, switching frequencies and duty cycles are set within the ranges of 1–10 kHz and 0.3–0.7, respectively. In each test, both the switching frequency and duty cycle are firstly set to obtain a fixed voltage-boosting ratio. Afterwards the DC source outputs a linear rising voltage for 100 s, resulting a gradual increase of operating current up to 90 A. A commercial power analyser Tektronix PA3000 is adopted to collect real-time conducting loss data. Table 1 summarizes the main electrical specifications of the boost chopper circuit.

Figure 4 shows the measured and fitted results of superconducting losses P_{HTS} with different switching frequencies, duty

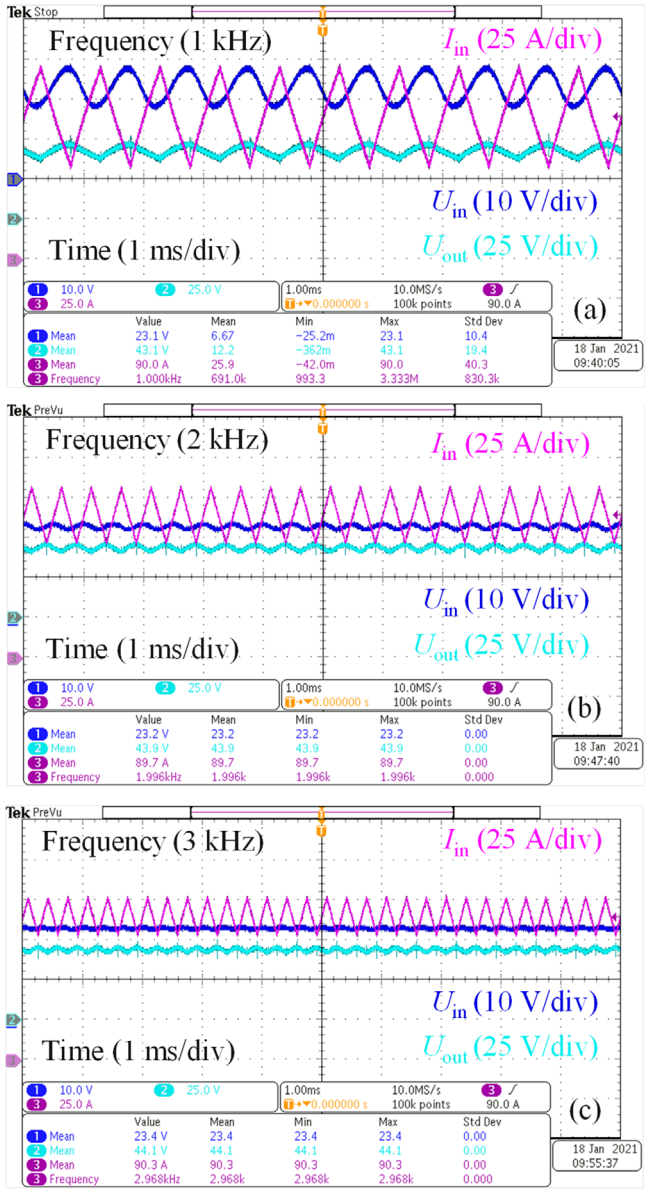

FIGURE 3 Experimental results of input/output voltages (U_{in},U_{out}) and inductor current I_{in} with different switching frequencies ($D = 0.5$, $I_{dc} = 90$ A, $R = 1\ \Omega$)

cycles and operating currents. It can be seen that overall trend of the measured data shows an exponential rising behaviour with the increase of operating current. To depict the mathematical relation between superconducting loss and operating current, a double-exponential function is fitted as follows:

$$P_{HTS} = p_1 \exp\left(p_2 I_{dc}\right) + p_3 \exp\left(p_4 I_{dc}\right) \tag{4}$$

where p_1 - p_4 are four fitted parameters depending on the switching frequency and duty cycle of PWM signal. For a fixed current of 90 A, the measured loss data shows an exponential damping behaviour with the increase of switching frequency and/or duty cycle. Therefore, a similar function in (4) can also be fitted in Figure 5 to match with the measured loss data by substituting the functional variables.

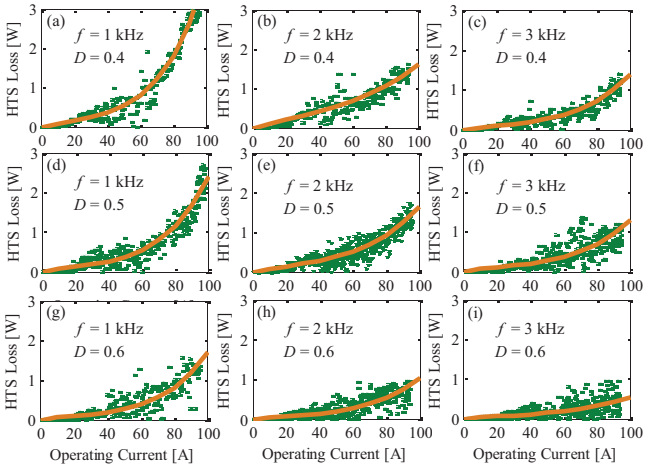

FIGURE 4 Measured and fitted results of superconducting losses with different switching frequencies, duty cycles and operating currents

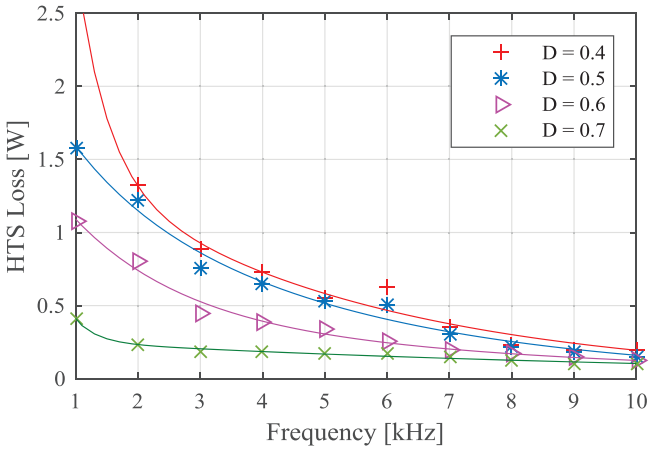

FIGURE 5 Measured and fitted results of superconducting losses with different switching frequencies and duty cycles (I_{dc} = 90 A)

From the data analyses above, two basic conclusions can be made as follows: (i) For a fixed current ripple factor, superconducting loss has a positive correlation with DC bias current; (ii) for a fixed DC bias current, superconducting loss has a negative correlation with both switching frequency and duty cycle. To summarize, the transient power dissipation in each switching cycle increases with the increase of DC current and/or AC ripple.

The losses in the superconducting inductor are measured with the frequency range 10–100 kHz. For the frequency increasing up to 100 kHz, the amplitude of current ripple gradually decreases. Basically, the loss of the superconducting inductor shows declining trend from the frequency 10 to 100 kHz, and there is no turning point, although there are some small fluctuations during the measurements at 15.6, 20.5, 34.1 kHz. However, the loss saturates when the frequency is over 60 kHz. One reason could be owing to the lower limit of measurable loss by the power analyser, and the other reason could be due to the dynamic equilibrium of the frequency and unit cycle loss. Meanwhile, with the increasing frequency, the

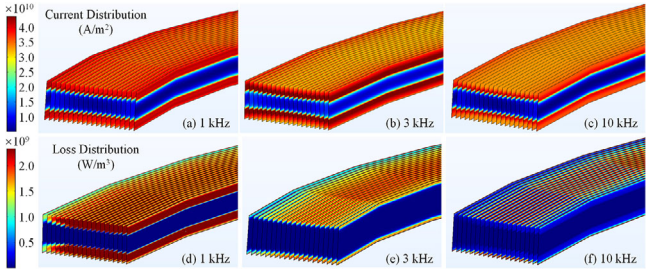

FIGURE 6 Peak current density and instantaneous superconducting loss distributions inside the superconducting inductor with the AC ripple frequencies of 1 kHz, 3 kHz and 10 kHz (I_{dc} = 90 A, D = 0.5)

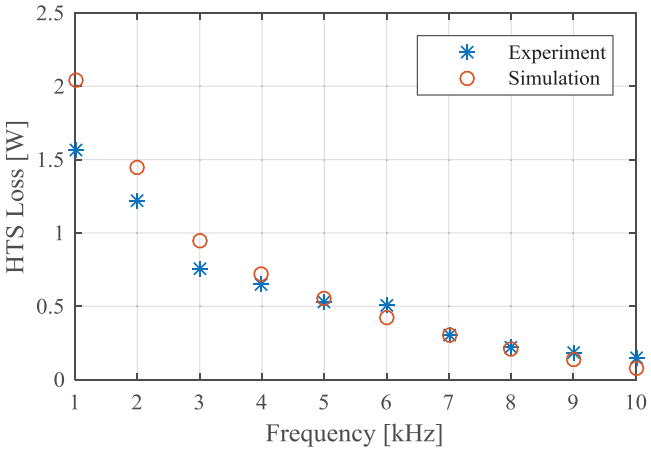

FIGURE 7 Comparison of simulation and experiment regarding the superconducting losses with different frequencies of the AC ripple current (I_{dc} = 90 A, D = 0.5)

chopper power MOSFETs suffer higher switching losses, which would weaken the overall efficiency of the chopper circuit. Consequently, considering both the losses from superconducting inductor and power switches, the operating frequency at 10 kHz is a reasonable choice for this circuit. We plan to further optimize and balance the losses from superconducting inductor and power switches, which can be beneficial to improve the overall efficiency of the cryogenic power electronic system in the future.

4 | SIMULATION ANALYSIS

Figure 6 shows the simulation results of peak current density and instantaneous total loss distributions inside the superconducting power inductor with the AC ripple frequencies of 1, 3 and 10 kHz. By comparison, the 1 kHz case in Figure 6a occupies the largest current density, because at relatively lower frequency the AC bias effect is stronger and leads to a higher peak transport current, while the 10 kHz case in Figure 6c carries much less peak transport current. Although the superconducting eddy-current loss is proportional to the square of frequency and the superconducting hysteresis loss has a linear relationship with the frequency [20], the total superconducting losses are decreasing notably with the increase of frequency, which can be clearly seen by comparing Figure 6d at 1 kHz and Figure 6f at 10 kHz. The main reason is due to the amplitude of AC ripple decreases remarkably with the increase of frequency, as the slope of the AC ripple is intrinsically unchanged. The much smaller AC ripple causes much less superconducting AC loss, and it could even minimise the superconducting dynamic loss as the induced AC field even could not reach the threshold field.

Figure 7 presents the comparison of simulation and experiment regarding the superconducting total losses. It can be seen that up to 30% difference are between the simulation and experiment with lower operating frequencies, which could attribute to that the power analyser could not handle the superconducting dynamic loss properly, while the simulation can provide reasonable values. However, when the operating frequency is high the simulation results are smaller than the measurement results, which could be due to the high frequency noise components could be more obvious with the small measurement signals. Overall, the simulation well matches the experiment. The skin effect in normal metals is important for higher frequency. However, the superconductor is different from the normal metals, and even for low frequency operation the current in the superconductor looks like having the "skin effect-like" phenomenon. As can be seen from the internal coated layer structure in Figure 1, the actual thickness of the superconducting layer is only 3–4 μm, which accounts for a very small proportion of the total thickness of the superconducting tape product (330 μm). Therefore, the "skin effect-like" phenomenon has already been well simulated by our advanced FEM model, and all the current has been properly verified to flow in the superconducting layer.

5 | PERFORMANCE COMPARISONS AND EVALUATIONS

In this work, a 200-μH class copper inductor is also made for the comparative analysis. To design a current rating of 100 A, six parallel enamelled copper wires with each wire having a diameter of 2.0 mm are used to wind 37 turns onto a cylinder-shaped magnetic core assembly. This core assembly is stacked directly by four Si-Fe magnetic powder cores KSF301026. The whole inductor has an average diameter of 90 mm and an average height of 85 mm, resulting in a total volume of about 540.75 cm^3 and a total weight of about 2.46 kg. Figure 8 shows the design configuration and device photo of a 200-μH class copper inductor. This copper inductor prototype is fabricated using typical engineering design methods, and its main electrical parameters including the current rating are also verified by experiments.

To further clarify the ultra-low-loss benefit of the superconducting inductor, the same testing conditions of operating currents, switching frequencies and duty cycles in Figures 4 and 5 are also applied to the copper inductor. Figure 9 shows the measurements and fitting results of the losses in the copper inductor with different switching frequencies and duty cycles (I_{dc} = 90 A). If comparing each set of the copper inductor losses in Figure 9 to the superconducting inductor losses in

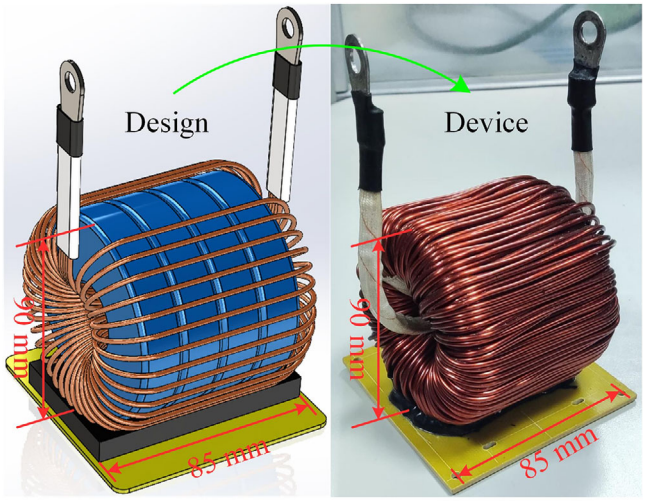

FIGURE 8 Design configuration and prototype photo of a copper inductor

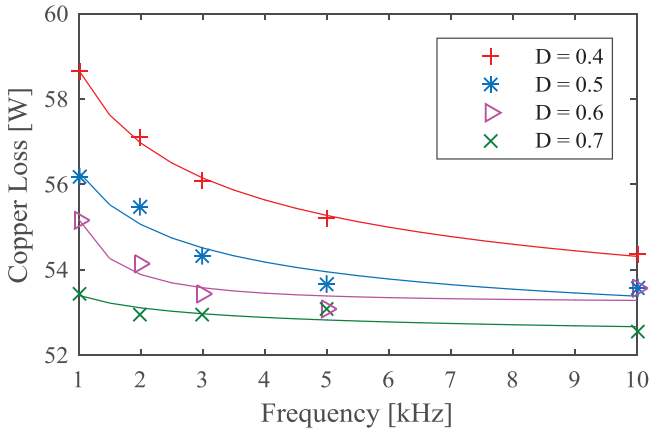

FIGURE 9 Measurements and fitting results of the losses in the copper inductor with different switching frequencies and duty cycles (I_{dc} = 90 A)

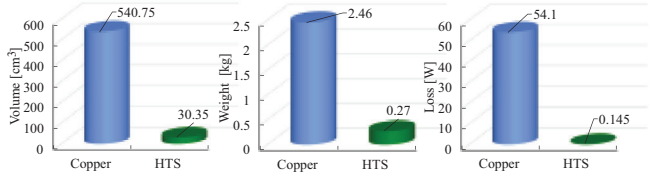

FIGURE 10 Comparison of 200-μH class superconducting inductor and copper inductor regarding the volume, weight and loss

Figure 5, tremendous advantages of superconducting inductor can be seen as the losses are generally over 100 times smaller and some are even more than 300 times smaller. Figure 10 also summarizes three main advantages of superconducting inductor as compared to the conventional inductor, it is much smaller (about 17 times) and lighter (about 9 times), and more importantly in that specific occasion it has much less loss (373 times smaller).

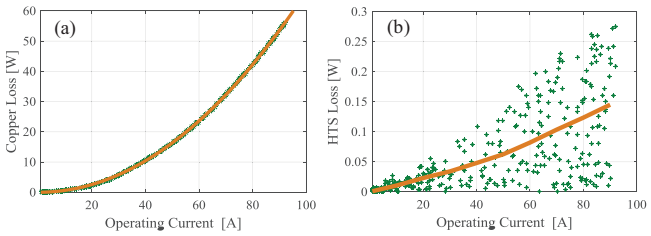

FIGURE 11 Measured and fitted results of (a) copper loss and (b) superconducting losses with different operating currents (f = 10 kHz, D = 0.5)

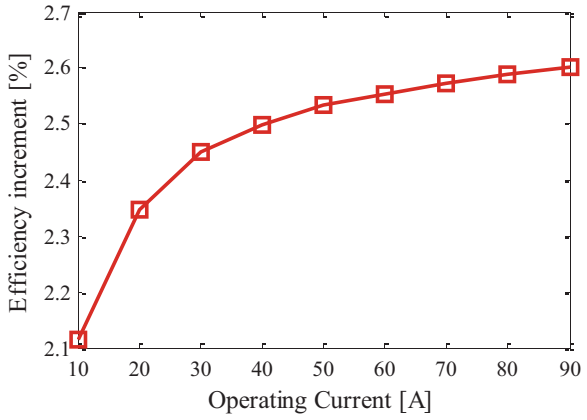

FIGURE 12 Increase in chopper efficiency when replacing the conventional copper inductor by the superconducting inductor (f = 10 kHz, D = 0.5)

Most measurements of the total losses are proportional to the square of the amplitude of the current flowing in the copper inductor. To be more precise, for a testing condition of f = 10 kHz and D = 0.5, the measured copper loss data is up to about 54.1 W at 90 A, as shown in Figure 11a. The corresponding equivalent lossy resistance is about 6.68 mΩ, which is slightly higher than the total DC resistance of 6.51 mΩ. This means that the winding loss actually counts for a significant majority of the total loss in this copper inductor. Unlike the copper winding having a relatively fixed lossy resistance, the total loss in the superconducting winding depends largely on the amplitude of AC ripple in each switching cycle, which has been convincingly proved by both experimental and numerical results in Sections 3 and 4. As shown in Figures 4d and 11b, under the same testing condition of I_{dc} = 90 A and D = 0.5, the total loss of the superconducting inductor decreases significantly from about 1575 mW at f = 1 kHz to about 145 mW at f = 10 kHz. By contrast, the superconducting loss measured at f = 10 kHz is only about 0.27% of that in the copper inductor. Despite a typical cryogenic cooling efficiency of 10% is considered [21], the actual power dissipation of the superconducting air-core inductor can be reduced significantly to about 2.7% compared to magnetic-core copper inductor. This means the proposed novel solution of replacing copper inductor by superconducting inductor can improve the operating efficiency of the chopper circuit if considering the substantial reduction in inductor loss. Figure 12 shows the increase in chopper efficiency with

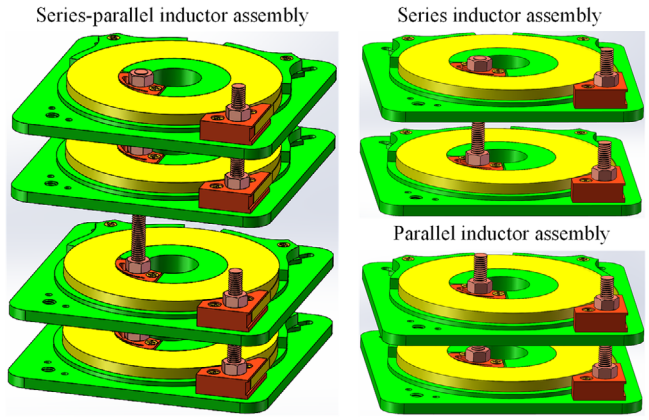

FIGURE 13 Three typical superconducting inductors assembled with pancake-shape units

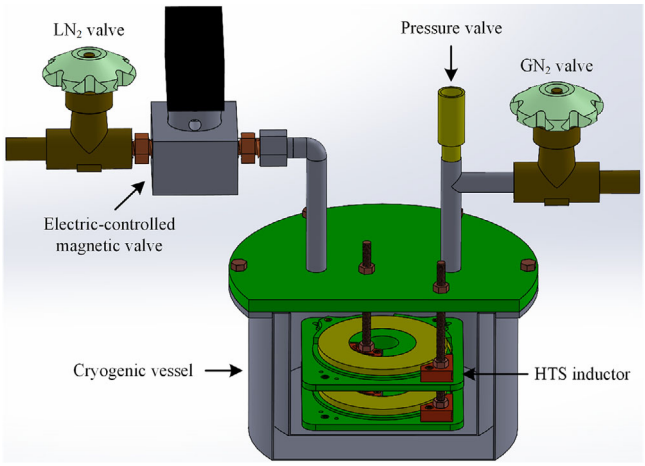

FIGURE 14 Compact and low-loss cryostat design for superconducting inductor in high-current power electronic applications

different operating currents. It can be seen that the overall efficiency improvement shows a gradual rising trend as the current increases. This is mainly because the HTS loss barely changes but the copper loss is proportional to the square of the operating current. For the case with an operating current 90 A and an output power 2 kW, the corresponding efficiency increment is up to 2.6% approximately in the experiment. Consequently, the superconducting inductor can well reduce the loss and improve the overall efficiency for high-current and high-power power electronic applications.

6 | PRACTICAL PROTOTYPE DESIGN AND COST ESTIMATION

The superconducting inductor is practical for a wide range of power electronic devices, from small-scale to large-scale applications. This article has already proved the superconducting inductor has been well acting as an inductive component in a lab-scale power electronic circuit, but also shows great advantages of much lower power loss (up to 373 times smaller) compared to conventional inductors. It is understandable that if engineers use superconducting inductors in high-power applications, the total inductance and its allowable operating current capacity should be larger as well. Taking another advantage of the compact geometry of the single superconducting inductor unit (only about 5 mm thick for the superconducting coil), they can be easily and efficiently stacked together and using the series connection or parallel connection, or series-parallel connection, as shown in the Figure 13. By using such configurations, the exact value of inductance can be realized and the overall size of the superconducting inductor can be still compact, which shows the flexibility of superconducting inductor towards different scales of power electronic applications.

The cryogenic environment of superconducting inductor is convenient to achieve as well. In this experiment, we used a small size liquid nitrogen container to accommodate the superconducting inductor. Merely about 10% occupancy was in the temperature 77 K, and major components (over 90%) were in the room temperature, as usual.

In order to further improve the practical feasibility of superconducting inductor to be equipped into different kinds of real power electronic devices, we developed a delicate cryostat (shown in Figure 14) for superconducting inductors, whose vessel is connected to the liquid nitrogen and gas nitrogen valves for the supply and circulation. The cost of the compact cryostat is about $100 and the overall cost of the superconducting inductor system is below $300. The cryostat has the advantages of compactness, low-loss, and low-cost. The total volume of the cryostat is only $0.18 \times 0.18 \times 0.1$ m^3, and it can contain 2 L liquid nitrogen. For instance, the total loss in the cryostat (heat dissipation and superconducting loss) is around 0.476 W, for a boost chopper circuit with 180 A current at 10 kHz. By calculation it uses 0.25 L liquid nitrogen (less than $0.5) per day, and the liquid nitrogen can be kept with proper level for 3–5 days and can be automatically refilled by the programmed and electric-controlled valve. If two copper inductors shown in Figure 8 are connected in parallel to achieve the current rating of 180 A, the total copper loss will be about 108. 2 W. Given a cooling efficiency of 10% [14], the actual power dissipation of the whole cryostat in Figure 14 is about 4.76 W. Then the corresponding efficiency increment is estimated to be about 2.55% when replacing the copper inductor by the proposed superconducting inductor with an advanced cryostat.

If the overall volume with the cryostat is considered, the size of the 200-μH superconducting inductor is larger than the copper inductor for this particular small power electronic circuit. However, it should be noticed that this merely a small-scale power electronic circuit, and for large-scale system the superconducting inductor can be much more advantageous. With the falling down price and the increasing production of superconducting materials, as well as the convenience of compact and low loss/cost cryogenic technology, it will be fully feasible that the superconducting inductor can be used by a great number of high-capacity power electronic applications such as the water electrolysis system [22, 23], photovoltaic power plant [24, 25], electric vehicle (EV) charging station [26, 27], and internal data

center [28, 29]. Most of these potential applications use low voltages but extremely high currents in the future low-carbon power and energy systems. This implies that a typical MW-class power conversion device might be operating with current level over 10 kA, which can be difficult to use conventional copper inductors with tremendous sizes.

The present solution mainly uses the parallel operation and combined control of up to several hundreds of power conversion units using conventional copper inductors [30–32]. This significantly enlarges the overall size of the integrated system, and also increases the investment of both the capital cost and operating cost. Worse, due to the system hardware redundancy and control complexity, conventional copper inductor based power conversion assemblies are more likely to suffer from the potential risk of power supply disturbances and faults. However, the compact power conversion unit using a high-current low-loss superconducting inductor can be expected to solve these issues and realize high-reliability power networks.

It should also be noted that the cryogenic operation of the power electronic switches like MOSFET has promising prospects because their reduced on-state resistances and improved energy efficiencies are better than the situations in the room temperature [33–35]. In particular, this so-called cryogenic power conversion is well suited to combine with our proposed superconducting inductor device which already has been using the proper self-contained cryogenic environments [36–38]. In addition to the significant efficiency improvement achieved by the uses of superconducting inductor and cryogenic power electronic switches, this emerging cryogenic power conversion technology also has the several accessary advantages as follows [21]: (1) Elimination of large-volume and heavy-weight drawbacks in conventional air or water cooled devices; (2) elimination of potential overheating risks in MOSFETs; (3) permission of high current and power ratings. Therefore, based on experimental and theoretical analyses on the high-efficiency superconducting inductor in this paper, and the loss characteristics of cryogenic power electronic switches in the literatures [33–38], there would be further balance and optimization of the operating parameters of superconductor elements and semiconductor devices in various cryogenic power conversion systems, with proper design guidelines [39-41].

7 | CONCLUSION

Experimental, theoretical and numerical investigations into the loss characteristics of a superconducting power electronic inductor have been presented. The results show that superconducting loss has a positive correlation with operating current, but negative correlation with both switching frequency and duty cycle. Two main superconducting losses, the superconducting AC loss and superconducting dynamic loss, have been accurately modelled based on the physical mechanisms, which have also verified that the experimental results are in reasonable ranges. Both the experiment and simulation show the loss from a superconducting inductor in the boost chopper circuit is reduced significantly up to 373 times lower than the loss from the magnetic-core copper inductor having the same conditions. Furthermore, the actual volume and weight of the superconducting inductor are only 5.61% and 10.97% of those of the copper inductor having the same inductance and current criteria.

A compact, low-loss and low-cost cryostat has been designed to accommodate the superconducting inductor, which can further improve the feasibility to introduce the superconducting inductor to be installed into various power electronic applications. The overall cost of the superconducting inductor together with the cryostat is below $300, and the maintenance is also cheap and simple and can be automatically done by the programmed and electric-controlled device. The new contents of this paper lay some technical bases for the wide uses of ultra-low-loss superconducting inductor into diverse high-dense high-power high-efficiency power electronic circuits and power conversion systems.

ACKNOWLEDGEMENT

This work was supported by the National Natural Science Foundation of China (51807128).

CONFLICT OF INTEREST

The authors declare that they have no known competing financial interests or personal relationships that could have appeared to influence the work reported in this article.

ORCID

Mingshun Zhang https://orcid.org/0000-0002-9149-5373
Boyang Shen https://orcid.org/0000-0001-8169-6588

REFERENCES

1. Sullivan, C.R., Reese, B.A., Stein, A.L., et al.: On size and magnetics: Why small efficient power inductors are rare. In: *2016 International Symposium on 3D Power Electronics Integration and Manufacturing (3D-PEIM)*. Raleigh, NC, pp. 1–23 (2016)
2. Hasanpour, S., Baghramian, A., Mojallali, H.: Analysis and modeling of a new coupled-inductor buck-boost DC-DC converter for renewable energy applications. IEEE Trans. Power Electron. 35(8), 8088–8101 (2020)
3. Calderon-Lopez, G., Scoltock, J., Wang, Y., et al.: Power-dense bidirectional DC–DC converters with high-performance inductors. IEEE Trans. Veh. Technol. 68(12), 11439–11448 (2019)
4. Yang, R.S., Hanson, A.J., Sullivan, C.R., et al.: Application flexibility of a low-loss high-frequency inductor structure. In: *2020 IEEE Applied Power Electronics Conference and Exposition (APEC)*. New Orleans, Louisiana, pp. 168–175 (2020)
5. Chen, R., Dong, Z., Zhang, Z., et al.: Core characterization and inductor design investigation at low temperature. In: *2018 IEEE Energy Conversion Congress and Exposition (ECCE)*. Portland, OR, pp. 4218–4225 (2018)
6. Claassen, J.H.: Inductor design for cryogenic power electronics. IEEE Trans. Appl. Supercond. 15(2), 2385–2388 (2005)
7. Chen, X.Y., Jin, J.X., Tang, M.G., et al.: An efficient boost chopper integrated with cryogenic MOSFETs and HTS inductor. IEEE Trans. Appl. Supercond. 26(7), 5701606 (2016)
8. Chen, X.Y., Zhang, M.S., Jiang, S., et al.: An SMES-based current-fed transformerless series voltage restorer for DC load protection. IEEE Trans. Power Electron. 36(9), 9698–9703 (2021)
9. Shen, B., Chen, Y., Li, C., et al.: Superconducting fault current limiter (SFCL): Experiment and the simulation from finite-element method (FEM) to power/energy system software. Energy 234, 121251 (2021)

10. Moradnouri, A., Ardeshiri, A., Vakilian, M., et al.: Survey on high-temperature superconducting transformer windings design. J. Supercond. Novel Magn. 33, 2581–2599 (2020)
11. Shen, B., Chen, X.Y., Liu, H., et al.: Quench protection modeling of an HTS magnet for MRI system. IEEE Trans. Appl. Supercond. 31(8), 4400705 (2021)
12. Schild, T., Libeyre, P., Bruton, A., et al.: Preparation of the ITER central solenoid assembly. IEEE Trans. Appl. Supercond. 30(4), 4201805 (2020)
13. Shen, B., Li, C., Geng, J., et al.: Power dissipation in HTS coated conductor coils under the simultaneous action of AC and DC currents and fields. Supercond. Sci. Technol. 31(7), 075005 (2018)
14. Grilli, F., Pardo, E., Stenvall, A., et al.: Computation of losses in HTS under the action of varying magnetic fields and currents. IEEE Trans. Appl. Supercond. 24(1), 78–110 (2014)
15. Shen, B., Grilli, F., Coombs, T.: Overview of H-formulation: A versatile tool for modelling electromagnetics in high-temperature superconductor applications. IEEE Access 8, 100403–100414 (2020)
16. Shen, B., Grilli, F., Coombs, T.: Review of the AC loss computation for HTS using H formulation. Supercond. Sci. Technol. 33(3), 033002 (2020)
17. Oomen, M.P., Rieger, J., Leghissa, M., et al.: Dynamic resistance in a slab-like superconductor with $J_c(B)$ dependence. Supercond. Sci. Technol. 12(6), 382–387 (1999)
18. Geng, J., Matsuda, K., Fu, L., et al.: Operational research on a high-T_c rectifier-type superconducting flux pump. Supercond. Sci. Technol. 29(3), 035015 (2016)
19. Ainslie, M.D., Bumby, C.W., Jiang, Z., et al.: Numerical modelling of dynamic resistance in high-temperature superconducting coated-conductor wires. Supercond. Sci. Technol. 31(7), 074003 (2018)
20. Shen, B., Li, J., Geng, J., et al.: Investigation and comparison of AC losses on stabilizer-free and copper stabilizer HTS tapes. Phys. C: Supercond. 541, 40–44 (2017)
21. Chen, Y., Chen, X.Y., Li, T., et al.: Experimental investigations of state-of-the-art 650-V class power MOSFETs for cryogenic power conversion at 77K. IEEE J. Electron Devices Soc. 6(1), 8–18 (2018)
22. Chen, X.Y., Chen, Y., Zhang, M., et al.: Hospital-oriented quad-generation (HOQG)—A combined cooling, heating, power and gas (CCHPG) system. Appl. Energy 300, 117382 (2021)
23. Wu, Q., Hu, Q., Hang, L., et al.: Power to gas for future renewable based energy systems. IET Renewable Power Gener. 14(17), 3281–3283 (2021)
24. Benda, V.: Photovoltaics towards terawatts–progress in photovoltaic cells and modules. IET Power Electron. 8(12), 2343–2351 (2015)
25. Zhang, D., Tang, S., Lin, B., et al.: Co-benefit of polycrystalline large-scale photovoltaic power in China. Energy 41(1), 436–442 (2012)
26. Joseph, P.K., Devaraj, E.: Design of hybrid forward boost converter for renewable energy powered electric vehicle charging applications. IET Power Electron. 12(8), 2015–2021 (2019)
27. Hussein, B., Abdi, N., Massoud, A.: Development of a three-phase interleaved converter based on SEPIC DC-DC converter operating in discontinuous conduction mode for ultra-fast electric vehicle charging stations. IET Power Electron., 14(11), 1889–1903 (2021)
28. He, J., Xiao, X., Zhong, R., et al.: New AC & DC hybrid power supply system and its reliability analysis in data centre. J. Eng. 2019(16), 2800–2803 (2019)
29. Kang, W.T., He, K., Lei, Y., et al.: A novel LVDC superconducting power distribution system for data center with power quality improvement and loss reduction. IEEE Trans. Appl. Supercond. 31(8), 1–4 (2021). https://doi.org/10.1109/TASC.2021.3103709
30. Chen, Y., Wang, H., Zhu, M., et al.: Modular DC-DC auto-transformer: Topology, operation, and system design. IET Power Electron. 14(13), 2289–2302 (2021)
31. Abrehdari, M., Sarvi, M.: Comprehensive sharing control strategy for input-series output-parallel connected modular DC–DC converters. IET Power Electron. 12(12), 3105–3117 (2019)
32. Kim, K.T., Kwon, J.M., Kwon, B.H.: Parallel operation of photovoltaic power conditioning system modules for large-scale photovoltaic power generation. IET Power Electron. 7(2), 406–417 (2014)
33. Luo, C., Li, Z., Lu, T.T., Xu, J., Guo, G.P.: MOSFET characterization and modeling at cryogenic temperatures. Cryogenics 98, 12–17 (2019)
34. Abd El-Azeem, S.M., El-Ghanam, S.M.: Comparative study of gallium nitride and silicon carbide MOSFETs as power switching applications under cryogenic conditions. Cryogenics 107, 103071 (2020)
35. Chen, X.Y., Jiang, S., Chen, Y., Gou, H.Y., Xie, Q., Shen, B.Y.: Transient modeling and loss analysis of SiC MOSFETs at cryogenic and room temperatures. IEEE Trans. Appl. Supercond. 31(8), 1400404 (2021)
36. Rajashekara, K., Akin, B.: Cryogenic power conversion systems: The next step in the evolution of power electronics technology. IEEE Electrif. Mag. 1(2), 64–73 (2013)
37. Bailey, W., Wen, H., Yang, Y., Forsyth, A., Jia, C.: A cryogenic dc-dc power converter for a 100 kW synchronous HTS generator at liquid nitrogen temperatures. Phys. Procedia 36, 1002–1007 (2012)
38. Forsyth, A.J., Jia, C., Wu, D., Tan, C.H., Dimler, S., Yang, Y., Bailey, W.: Cryogenic converter for superconducting coil control. IET Power Electron. 5(6), 739–746 (2012)
39. Chen X., Jiang S., Chen Y., Zou Z., Shen B., Lei Y., Zhang D., Zhang M., Gou H.: Energy-saving superconducting power delivery from renewable energy source to a 100-MW-class data center. Applied Energy. 310, 118602 (2022).
40. Chen X., Pang Z., Gou H., Xie Q., Zhao R., Shi Z., Shen B.: Intelligent design of large-size HTS magnets for SMES and high-field applications: using a self-programmed GUI tool. Superconductor Science and Technology, 34(9), 095008 (2021).
41. Chen X., Gou H., Chen Y., Jiang S., Zhang M., Pang Z., Shen B.: Superconducting fault current limiter (SFCL) for a power electronic circuit: experiment and numerical modelling. Superconductor Science and Technology, 35(4), 045010 (2022).

How to cite this article: Chen, X., Gou, H., Chen, Y., Zeng, L., Zhang, M., Jiang, S., Xie, Q., Shen, B.: An ultra-low-loss superconducting inductor for power electronic circuits. IET Power Electron. 1–9 (2022). https://doi.org/10.1049/pel2.12275